Available online at www.sciencedirect.com
SCIENCE DIRECT®
Physics Letters B 611 (2005) 231–238
PHYSICS LETTERS B
www.elsevier.com/locate/physletb

Possible observation of photon speed energy dependence

V. Gharibyan

Yerevan Physics Institute, Armenia

Received 10 July 2004; accepted 24 February 2005

Editor: M. Doser

Abstract

Current constraints on photon velocity variability are summarized and displayed in terms of an energy-dependent vacuum refraction index. It is shown that the energy–momentum balance of high energy Compton scattering is very sensitive to the outgoing photon speed. A missing energy observation in HERA Compton polarimeter data indicates that photons with 12.7 GeV energy are moving faster than light by 5.1(1.4) mm/s. An asymmetry spectrum measured by the SLC longitudinal polarimeter implies however an effect which is 42 times smaller, although the interpretation of the data is less clear here.

PACS: 14.70.Bh

Keywords: Photon speed; Compton scattering; Dispersive vacuum

1. Theoretical models

According to relativistic kinematics a photon velocity in vacuum c_γ does not depend on its energy ω, while a possible dependency is constrained by the current photon mass limit $m_\gamma < 10^{-16}$ eV [1] as $1 - c_\gamma(\omega)/c \leqslant 10^{-32}\omega^{-2}$ eV^2, where c is a massless particle vacuum speed. However, the laboratory or stellar vacuum always contains background fields (matter) and quantum interactions can slow down or speed up photon propagation. Tiny changes of the photon velocity have been predicted [2,3] for such nontrivial, polarized vacua modified by electromagnetic or gravitational fields, temperature or boundary conditions within the perturbative quantum electrodynamics which allows to derive inverse relative velocities (vacuum refraction indices $n = c/c_\gamma$) mainly for low energy $\omega \ll m$ (m is the electron mass) photons [4]. Even in the absence of background fields vacuum quantum fluctuations can influence light propagation as pointed out for the gravitational vacuum by recent developments in quantum gravity theory [5(a)–(c)]. Changes of photon speed are expected to be significant at photon energies close to the Planck mass $\approx 10^{19}$ GeV decreasing with lower energies. Hypothetical Lorentz

E-mail address: vaagn@mail.desy.de (V. Gharibyan).

0370-2693/$ – see front matter © 2005 Published by Elsevier B.V.
doi:10.1016/j.physletb.2005.02.053

symmetry deformations considered for explaining the observed ultrahigh energy cosmic rays above the GZK cutoff (and possibly neutrino oscillations) [6] may also introduce an energy-dependent photon speed [7].

2. Experimental limits

Magnitudes of these predicted effects are small and though may exceed by many orders the constraints imposed by the photon mass, all experimental tests so far show that different energy photons in vacuum move at the same velocity (light vacuum speed c) within the constraints displayed on Fig. 1 (use of vacuum refraction index $n(\omega)$ instead of photon velocity is convenient to distinguish between photon mass and vacuum properties).

The most stringent limits are coming from the detection of highest energy proton and γ cosmic particles as first noted in [8], since in a dispersive vacuum they would quickly decay by vacuum Cherenkov radiation $p \to p\gamma$ ($n > 1$) and pair creation $\gamma \to e^+e^-$ ($n < 1$). These processes are kinematically forbidden in case

$$n - 1 < \frac{M^2}{2E^2 - 2\omega E - M^2},$$
$$1 - n < \frac{2m^2}{\omega^2} \tag{1}$$

for Cherenkov radiation and pair creation, respectively, with M, E the proton mass and energy. Excluded areas in Fig. 1 correspond to a highest detected proton energy of $E = 10^{20}$ eV [9] and to a cosmic photon spectrum up to $\omega_{\max} = 22$ TeV [10]. Also shown is a limit inferred from the highest observed electron energy of 2 TeV [11]. Other areas are excluded by experiments utilizing direct time of flight techniques sensitive to $|n - 1| \approx \Delta t c/D$, where Δt is a time difference between arrivals of simultaneously emitted photons with different energy and D is a distance to the source. While laboratory experiments are limited by time resolutions of typically a few picoseconds and distances of a few kilometers (an early SLAC result [12] $|n - 1| < 2 \times 10^{-7}$ is shown on Fig. 1 by a narrow white bar at 15 GeV $< \omega <$ 20 GeV) the astrophysical observations could do much better owing to huge distances to the source. In Ref. [13] one can find limits on light speed variations in wide energy ranges

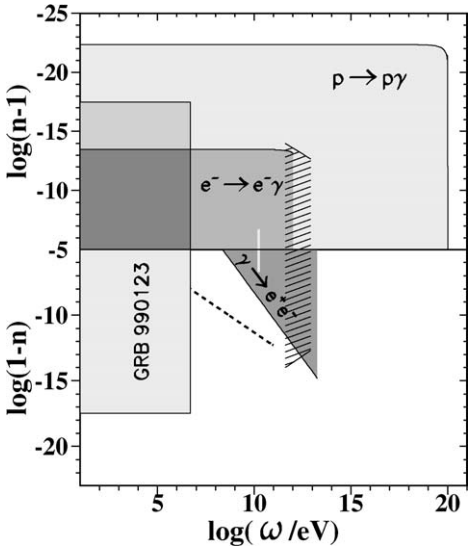

Fig. 1. Experimental constraints on the vacuum refraction index.

based on different astrophysical events; these limits suffer, however, from very uncertain distance scales. Meanwhile an observed spectacular gamma ray burst GRB990123 [14] followed by an optical counterpart detected within $\Delta t = 22$ s, with a distance $z = 1.6$, could establish a constraint $|n - 1| < 3 \times 10^{-18}$ for 2 eV $< \omega <$ 5 MeV, which is anyhow the order of constraints quoted in Ref. [13]. Photons with highest observed energies 0.35 TeV $< \omega <$ 10 TeV from a well defined active galaxy source (Markarian 421) put constraints $|n - 1| < 2.5 \times 10^{-17}\omega$ [15] (hatched area in Fig. 1).

3. Compton scattering in dispersive vacuum

Apart from the discussed threshold effects for vacuum Cherenkov and pair creation, the dispersive vacuum will modify the kinematics of other processes involving free photons according to the dispersion relation $k^2 = \omega^2(1 - n^2)$. However, the tiny refraction imposed by such vacuum becomes observable only at high energies with corresponding small angles. When the photon (four-momentum k) interacts with a particle (four-momentum P) the vacuum index will contribute to the convolution Pk as

$$Pk \approx \frac{\mathcal{E}\omega}{2}\left(\frac{1}{\gamma^2} + \theta^2 + 2(1 - n)\right) \tag{2}$$

where $\mathcal{E}$, $\gamma \gg 1$ are energy, Lorentz-factor of the particle, and $\theta \ll 1$ is the angle between the photon and the particle. Thus, such processes in general could detect a relative photon speed variation, at given energy ω, as small as the order of $1/2\gamma^2$.

Below we concentrate on photon scattering off an ultrarelativistic electron and apply (2) in energy–momentum conservation to get sensitivity of the high energy Compton process to the vacuum refraction index. If $\omega_0, \theta_0, \omega, \theta$ designate energy and angle of the incident and scattered photons, for $\omega_0 \ll \omega$, $m \ll \omega$ we have

$$n - 1 = \frac{1}{2\gamma^2}\left[1 + \theta^2\gamma^2 - x\left(\frac{\mathcal{E}}{\omega} - 1\right)\right], \tag{3}$$

where γ, $\mathcal{E}$ are the Lorentz-factor and energy of the initial electron,

$$x \equiv \frac{4\gamma\omega_0 \sin^2(\theta_0/2)}{m},$$

and n is the index for the direction θ and energy ω. In a case of laser Compton scattering on accelerator electrons the initial states (x, γ) are known to high degree of precision (typically to 0.01%) which allows to gain information about n from each event measuring the ω and θ (or the energy and angle of the scattered electron $\mathcal{E}'$, θ', since $\omega = \mathcal{E} - \mathcal{E}'$, $\theta = \theta'\mathcal{E}'/\omega$). Alternatively, one could detect only the Compton edge, i.e., maximal (minimal) energy of the scattered photons (electrons) $\omega_m \equiv \omega$ at $\theta = 0$ ($\mathcal{E}'_m \equiv \mathcal{E} - \omega_m$) to measure n (ω_m) down to values of

$$|n - 1| \leqslant \frac{2\omega_0}{\omega_m}\frac{\Delta\omega_m}{\omega_m}, \tag{4}$$

which follows from (3) if ω_m is measured with relative uncertainty $\Delta\omega_m/\omega_m$. A dotted line in Fig. 1 shows the potential of laboratory Compton scattering in limiting n according to (4) for optical lasers ($\omega_0 \approx 2$ eV) with a modest precision $\Delta\omega_m/\omega_m = 1\%$ up to a photon energy of 100 GeV.

The laser scattering is particularly attractive to test vacuum birefringence since the highest energy scattered photons preserve the laser polarization [16] which is easy to change. Flipping the laser linear polarization one could measure $n_\perp$, $n_\parallel$ components for multi-GeV photons by detecting the Compton edge dependence on $\perp$, $\parallel$ polarization states (current bounds on the vacuum birefringence [17] are set by polarimetry of (near)optical photons coming from distant astronomical sources).

In Ref. [18] it has been proposed to test different quantities related to photon velocity by high energy Compton process measuring simultaneously the scattered photon and electron energies. However, this set of measurements is not sensitive to the photon speed which is accessible only from the photon energy and momentum combined information. To measure the photon momentum one has to register scattering angle of the photon or electron relying for the latter case on energy–momentum conservation. It is possible to indirectly register zero scattering angle of the photon by detecting the Compton edge as it pointed out above and only then an energy measurement alone is sufficient to obtain information about the photon speed. Another distinguished kinematic point in the Compton process, where circularly polarized photons interact with longitudinally polarized electrons, is the energy asymmetry (between spin 1/2 and 3/2 states) zero crossing which occurs at the maximal scattering angle of the electron and therefore at a fixed photon momentum. Thus, the corresponding energy $\omega_{A=0}$ of the scattered photon gives a measure of the photon speed

$$n - 1 = \frac{1}{2\gamma^2}\left[1 - \frac{x}{2}\left(\frac{\mathcal{E}}{\omega_{A=0}} - 1\right)\right]. \tag{5}$$

This is a reduced form of Eq. (3) where angle detection is replaced by an energy measurement at the expense of dealing with polarized beams and is useful because most of the laboratory Compton devices are working as polarimeters.

Derived relations allow to extract the refraction index and associated photon speed from existing polarimetric data.

4. HERA polarimeter spectra analysis

Consider photon spectra (Fig. 2) from Ref. [19] measured by the HERA Compton polarimeter. The spectra were obtained by directing a CW 514.5 nm laser light against the HERA transversely polarized, 26.5 GeV electron beam with a vertical crossing angle of 3.1 mrad and detecting produced high energy γ-quanta with a sampling calorimeter. The whole detection scheme is designed for measurement of an up–down spatial asymmetry of the γ-quanta which is

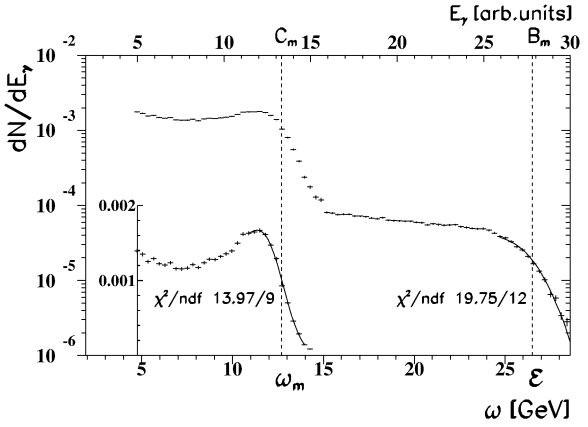

Fig. 2. HERA polarimeter Compton events on top of background Bremsstrahlung and background subtracted Compton spectrum (inset) with fit results. Upper scale: original energy calibration using nominal Compton edge (GeV replaced by arb. units). Lower scale: recalibration using Bremsstrahlung edge.

introduced by a flip of the laser light helicity and is proportional to the electron beam polarization while the energy measurement is auxiliary and serves as a mean to enhance the asymmetry by proper energy cuts. We are going to extract Compton γ's maximal energy from the spectra and estimate the refraction index via Eq. (3) at $\theta = 0$. Hence, following [19,20], we concentrate on details of the experimental setup important for energy measurement only, ignoring all features related to polarization.

The scattered Compton photons originate from an interaction region (IR) about 50 cm long, defined by the crossing angle and size of the electron and laser beams. Bending magnets downstream of the IR separate the electron and γ beams and the photons leave the vacuum pipe through a 0.5 mm thick aluminum window to pass 39 m of air before entering the calorimeter which is installed 65 m away from the IR.

Collimators placed at a distance of 47 m from the IR, define an aperture of ± 0.37 mrad the same as angular size of the calorimeter as seen from the IR. The aperture is 15 times larger than the largest (horizontal) angular spread of electrons at the IR and 40 times larger than the characteristic radiation angle $1/\gamma$ so the acceptance inefficiency can be ignored. The collimators are followed by magnets to sweep out charged background.

The calorimeter consists of 12 layers of 6.2 mm thick tungsten and 2.6 mm thick scintillator plates surrounded by 4 wavelength shifters attached to 4 photomultipliers. PMT signals from single photons are integrated within 100 ns gate then digitized with 12 bit ADCs and gains of the PMTs are adjusted to about 15 MeV per ADC channel. A fast DAQ handles the signals and operates without dead time up to an average data rate of 100 kHz. The detector performance has been simulated with EGS4 Monte Carlo program and tested using DESY and CERN test beams. Measured energy resolution of 24% $\mathrm{GeV}^{1/2}$, spatial nonuniformity of $\pm 1\%$ and nonlinearity of 2% at 20 GeV are reported to be in agreement with the simulations.

Apart from the laser light, the electron beam also interacts with residual gas, thermal photons and bending magnetic field in the beam pipe producing respectively Bremsstrahlung, scattered blackbody and synchrotron radiation reaching the calorimeter. To measure this background the laser beam is blocked for 20 s of each 1 min measurement cycle (light on/off is 40/20 s). The procedure allows to eliminate the background by a simple subtraction of time normalized light-off spectrum from the light-on spectrum. Exact on/off durations are counted by DAQ clocks.

At the time of the measurements an electron beam current of 0.32 mA and a laser power of 10 W provide 1 kHz rate above an energy threshold of 1.75 GeV while the background rate was 0.15 kHz. With such high threshold only the Bremsstrahlung contributes to background since the scattered blackbody radiation maximal energy is 0.73 GeV and the synchrotron radiation is absorbed in the first tungsten plate of the calorimeter.

Putting the laser photon, HERA electron energy and the crossing angle ($\omega_0 = 2.41$ eV, $\mathcal{E} = 26.5$ GeV, $\theta_0 = \pi + 3.1$ mrad) into the definition of the kinematic parameter x, we get $x = 0.9783$. The precision of the parameter is limited by the electron beam energy uncertainty $\sigma(\mathcal{E})/\mathcal{E} \approx 10^{-4}$. Errors of the other constituents $\sigma(\omega_0)/\omega_0 \approx 10^{-5}$, $\sigma(m)/m \approx 3 \times 10^{-7}$, $\Delta(\theta_0) \approx 2$ mrad $\Rightarrow \Delta \sin^2(\theta_0/2) \approx 3 \times 10^{-6}$ contribute negligibly.

To measure the ratio $\mathcal{E}/\omega_m$ (the only unknown in the right part of (3) at $\theta = 0$) we can utilize the Bremsstrahlung spectrum [19, Fig. 18] which helps to cancel the absolute energy calibration of the calorimeter since

$$\frac{\mathcal{E}}{\omega_m} = \frac{\alpha B_m + m}{\alpha C_m} = \frac{B_m}{C_m} + O\left(4 \times 10^{-5}\right), \tag{6}$$

where α is a calibration constant and B_m, C_m are the Bremsstrahlung and Compton edges derived from the measured spectra in arbitrary units. It is easy to verify that influence of the term (2) to the Bremsstrahlung maximal energy is negligible, i.e., a non-zero $|n-1|$ shifts only the Compton edge.

A spectrum measured via calorimetry is conventionally described by a function

$$F(E_\gamma) = N \int_0^{E_m} \frac{d\Sigma}{d\omega} \frac{1}{\sqrt{\omega}} \exp\left(\frac{-(\omega - E_\gamma)^2}{2\sigma_0^2 \omega}\right) d\omega, \quad (7)$$

where a parent energy distribution $d\Sigma/d\omega$ incident on the detector is folded with a response function which is a Gaussian with energy-dependent width equal to the calorimeter energy resolution (in our case $\sigma_0 = 0.24\ \mathrm{GeV}^{1/2}$), N is a normalization constant and E_m is the cutoff energy of the parent distribution.

The original energy calibration is made to match the nominal Compton edge $\mathcal{E}x/(1+x) = 13.10$ GeV (Fig. 2, upper scale) by applying a differentiation deconvolution method to find the cutoff energy. This method unfolds the spectrum by numerical differentiation to reveal a nearly Gaussian peak (inverted) within the spectrum fall-off range and assigns the peak position to the cutoff value. The main drawback of this method comes from ignorance of the parent distribution which results in a shifted answer in case of non-flat distributions as follows from (7). Therefore, to extract the B_m, C_m values from the spectra we have used a more precise approach (fitting via (7)) and have applied the differentiation method only to find the fit ranges around end points where the differentiated spectra peak, since outside of these ranges the spectra contain no information about the cutoff energies. Such localization also helps to avoid possible bias of the fit results caused by physical effects affecting the spectra and not entering in the function $F(E_\gamma)$. Dominating among these effects are photon conversions between the interaction point and the calorimeter, detector nonlinearity and spatial non-uniform response. These effects change the shape of the spectra in a way the function (7) is not able to describe adequately over the full energy range which is expressed also in Ref. [19] and is noticeable for original fits shown on Fig. 18 and Fig. 21 of [19].

Fitting the function $F(E_\gamma)$ to the background spectrum with the beam-gas Bremsstrahlung cross-section [21] as the parent distribution and 2 free, variable parameters E_m, N, we get $E_m = 27.799 \pm 0.047 = B_m$ (see Fig. 2). The fit range is predefined by numerical differentiation of the spectrum as discussed above. From a similar fit to the background subtracted Compton spectrum (from Fig. 21 of Ref. [19]) by $F(E_\gamma)$ with the Compton cross-section [22] as parent distribution, we find $E_m = 13.322 \pm 0.010 = C_m$ (Fig. 2 inset). According to the derived numbers B_m, C_m and relations (6), (3) we have the Compton edge at $\omega_m = 12.70 \pm 0.02$ GeV, well below from the nominal $\omega_m(n=1) = 13.10$ GeV value and a vacuum index for the 12.7 GeV photons $n = 1 - (1.17 \pm 0.07) \times 10^{-11}$ which is responsible for such reduction.

Now we return to the above-mentioned systematic effects to estimate their possible influence on the obtained cutoff energies. The non-evacuated path of γ beam line serves as an extended target to convert them into e^+e^- pairs, subject to continuous energy loss and multiple scattering before registration by the calorimeter. This modifies the spectra by enhancing lower energy parts without affecting the highest detected energies from non-converted γ-quanta. The most significant instrumental source affecting the result is the detector non-linear response $E\alpha^{-1}(1+fE)$ under a given energy E with $f = -0.001\ \mathrm{GeV}^{-1}$ from the quoted nonlinearity of 2% at $E = 20$ GeV ($f < 0$ corresponds to a conventional calorimetric nonlinearity arising from shower leakage). This brings the ratio (6) to

$$\frac{B_m}{C_m} \approx \frac{\mathcal{E}}{\omega_m}\big(1 + f(\mathcal{E} - \omega_m)\big) \quad (8)$$

with a corresponding correction of 0.52×10^{-11} for n and half of that value as the correction error.

Another possible source of the edges mismatch would arise if the Bremsstrahlung and Compton beams incident on calorimeter are separated in space. Propagating the quoted spatial non-uniformity of the calorimeter $\pm 1\%$ ($B_m/C_m \to B_m/C_m(1 \pm 0.01)$) to the value of n we finally have

$$n = 1 - (1.69 \pm 0.07 \pm 0.38 \pm 0.26) \times 10^{-11}$$

with statistical and systematic non-uniformity, nonlinearity errors displayed separately.

For completeness of the analysis, we discuss a few additional systematic sources which have no significant effect on the energy distributions. First is

the ADC electronic pedestal with a width equal to ≈ 30 MeV and a measured systematic shift of the mean of ± 4 MeV. This is neglected, since the pedestal spread is incorporated into the energy resolution while the shift is less than the result's smallest, statistical error by almost one order of magnitude. Next is an emission of multiple photons by a single electron bunch resulting in enhanced maximal detected energies due to a pile-up in the calorimeter. Using a Poisson distribution and evaluating the quoted single photon emission probability $p_C(1) = 0.02$ at the given Compton rate, one readily has probabilities for 2 photon emission $p_C(2) = 2.2 \times 10^{-4}$ and $p_B(2) = 9.9 \times 10^{-6}$ for Compton and Bremsstrahlung, respectively. The latter number is too small to cause any considerable shift of B_m, since the whole Bremsstrahlung spectrum contains less than a few pile-up events. Concerning the Compton edge, correcting for pile-up would only aggravate the observed energy reduction. The same is true also for non-linear Compton scattering events where an electron emits two or more photons at once.

5. SLC polarimeter asymmetry analysis

In Ref. [23] one can find a Compton asymmetry (Fig. 3) measured by the SLC polarimeter where high power laser pulses of 532 nm circular light interact with longitudinally polarized bunches of 45.6 GeV electrons under a crossing angle of 10 mrad and recoil electrons are registered by an array of Cherenkov counters installed downstream of two momentum analyzing bending magnets. Each channel of the detector integrates multiple electrons per pulse, within a certain energy range according to its position in the array. Following a detailed description of the polarimeter setup in [24] one infers that energies detected in the Nth channel are constrained by

$$\mathcal{E}'_{\min(\max)} = C_0\big(S_N + (-)D/2 + S - S_c\big)^{-1}, \qquad (9)$$

where $C_0 = 296.45$ GeV cm, $S = 10.58$ cm, $S_N = N$ cm, $D = 1$ cm which is the channel size and S_c is the Compton kinematic endpoint distance from the channel 7 inner edge which also depends on the initial electron beam position relative to the detector. Information about the photon speed is encoded into the relation of the Compton maximal and asymmetry zero crossing energies according to Eq. (5). A coarse

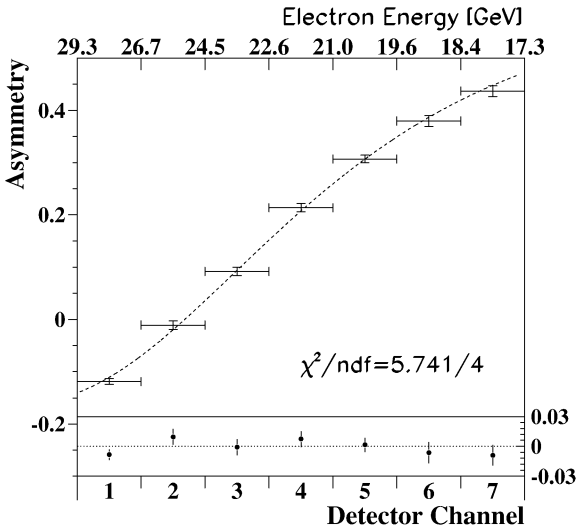

Fig. 3. SLC polarimeter asymmetry (lower scale) with fit results (upper scale). The dotted line shows the parent distribution $d\Sigma_\lambda/d\Sigma_c$. The lower part displays the fit residuals (right scale).

granularity of the detector (binning in Fig. 3), however, makes it difficult to apply this simple kinematic method. Instead one can utilize dynamic features of the Compton scattering in the case of $n \neq 1$. Using an invariant representation of the Compton process in Ref. [22], for longitudinal polarization of the incident electron beam one can write the cross-section as

$$\frac{d\Sigma_c}{dy} + \lambda\frac{d\Sigma_\lambda}{dy} = \frac{\pi r_e^2}{x}\left(\frac{1}{1-y} + 1 - y - 4r(1-r) + \lambda u\right), \qquad (10)$$

where r_e is the classical electron radius, λ is the electron beam and circular light polarizations product, $r = y/(x-xy)$, $u = rx(1-2r)(2-y)$, $y = 1 - Pk/Pk_0$ with k_0 being the photon's initial four-momentum, and $x = 2Pk_0/m^2$, which is the kinematic parameter defined above.

To introduce a refraction index into the cross-section, we modify Pk entering in y according to (2) and scale cross-section (10) by a factor of

$$\left(n^2 + n\omega\frac{dn}{d\omega}\right)^{-1},$$

which accounts for a change of the delta function $\delta(\omega^2 - \mathbf{k}^2)$ to $\delta(n^2\omega^2 - \mathbf{k}^2)$ in the phase space of the outgoing photon. In addition we use (3) and en-

ergy conservation to eliminate θ and express the cross-section in terms of $\mathcal{E}'$.

The asymmetry A_N measured in a given detector channel N is a product of λ and an analyzing power I_λ/I_c ($A_N = \lambda I_\lambda/I_c$), where

$$I_{\lambda(c)} = \int_{\mathcal{E}'_{\min}}^{\mathcal{E}'_{\max}} \mathcal{E}' \frac{d\Sigma_{\lambda(c)}}{d\mathcal{E}'} d\mathcal{E}' \tag{11}$$

with $\mathcal{E}'$ being the scattered electron energy limited by the channel's energy acceptance $\mathcal{E}'_{\min}$, $\mathcal{E}'_{\max}$.

It follows from (9)–(11) that in the case of $n = 1$, the parameters S_c and λ establish horizontal and vertical scales (energy and asymmetry), respectively, in Fig. 3. However, these variables alone are not sufficient for a satisfactory description of the asymmetry distribution as indicated by a least squares fit performed with only two free parameters S_c and λ. Ref. [24] also reports about interchannel inconsistencies which dictate the choice and use of only one channel (number 7) for the polarization measurement.

To extract the photon speed we add one more free parameter $\psi \equiv 2\gamma^2(n-1)$ and use the polarized Compton cross-section modified by dispersion, assuming a constant refraction index across the entire energy range of the measured asymmetry. Now the χ^2 minimization converges with $\lambda = 0.628 \pm 0.009$, $S_c = 0.970 \pm 0.037$ and $\psi = -(6.49 \pm 0.08) \times 10^{-3}$ (Fig. 3), which yields

$$n = 1 - (4.07 \pm 0.05) \times 10^{-13}$$

for photons in the energy range $16.3\,\text{GeV} < \omega < 28.3\,\text{GeV}$.

An influence of the detector response on the asymmetry is quoted in [24] to be about 1%, which is much smaller than statistical fluctuations and we ignore it. Assuming perfect circular polarization of the laser light, λ equals the electron beam polarization, which is measured to be 0.612 ± 0.014 from the channel 7 asymmetry. Both numbers agree within statistical and declared 1.41% systematic [24] errors, and at the same time the $n \neq 1$ hypothesis allowed the asymmetry spectrum to be fitted successfully.

Although the obtained result is more precise compared to the HERA observation, it is less reliable because of the multi-electron generation–detection scheme and a theoretical uncertainty. The multi-particle mode, in general, poses difficulties to separate and treat the systematics and it also forced us to abandon the clear kinematic approach utilized in the case of the HERA polarimeter, while the method applied for modification of the Compton cross-section is somewhat heuristic and may introduce theoretical errors.

6. Discussion

The observed value of the index, obtained from one sample of the HERA polarimeter data, is statistically significant and does not contradict any previous experimental result (Fig. 1). It is below unity testifying that 12.7 GeV energy photons are moving faster than light (by $c(1-n) = 5.07 \pm 1.41$ mm/s). However, a SLAC experiment shows that for photons of energy 16.3–28.3 GeV, the departure from the speed of light is at most 0.122 ± 0.0015 mm/s.

Although the sign of the effect alone may be favorable for some theories discussed in Section 1, the detected magnitude is too large to be associated with polarized electromagnetic or gravitational vacuum. So, the outcome is unexpected, especially in view of the sharper limits for surrounding energies (see Fig. 1) and it is interesting to see whether the result can stand an examination by dedicated measurements and/or rigorous analysis of other pieces of data.

Acknowledgements

The author would like to thank A.T. Margarian for useful discussions and to M. Lomperski for providing measurement details and pointing to some sources of systematic uncertainties of the HERA polarimeter.

References

[1] D.E. Groom, et al., Particle Data Group Collaboration, Eur. Phys. J. C 15 (2000) 1.
[2] J.I. Latorre, P. Pascual, R. Tarrach, Nucl. Phys. B 437 (1995) 60, hep-th/9408016.
[3] W. Dittrich, H. Gies, Phys. Rev. D 58 (1998) 025004, hep-ph/9804375.
[4] K. Scharnhorst, Ann. Phys. 7 (1998) 700, hep-th/9810221.
[5] (a) G. Amelino-Camelia, J. Ellis, N.E. Mavromatos, D.V. Nanopoulos, S. Sarkar, Nature 393 (1998) 763;

(b) G. Amelino-Camelia, J. Ellis, N.E. Mavromatos, D.V. Nanopoulos, Int. J. Mod. Phys. A 12 (1997) 607;
(c) R. Gambini, J. Pullin, Phys. Rev. D 59 (1999) 124021, gr-qc/9809038.
[6] S. Coleman, S.L. Glashow, Phys. Rev. D 59 (1999) 116008, hep-ph/9812418.
[7] G. Amelino-Camelia, T. Piran, Phys. Rev. D 64 (2001) 036005, astro-ph/0008107.
[8] S. Coleman, S.L. Glashow, Phys. Lett. B 405 (1997) 249, hep-ph/9703240.
[9] J. Wdowczyk, A.W. Wolfendale, Annu. Rev. Nucl. Part. Sci. 39 (1989) 43.
[10] A. Konopelko, et al., HEGRA Collaboration, Astropart. Phys. 4 (1996) 199.
[11] T. Kobayashi, et al., Prepared for 26th International Cosmic Ray Conference (ICRC 99), Salt Lake City, UT, 17–25 August, 1999.
[12] Z.G. Guiragossian, G.B. Rothbart, M.R. Yearian, R. Gearhart, J.J. Murray, Phys. Rev. Lett. 34 (1975) 335.
[13] B.E. Schaefer, Phys. Rev. Lett. 82 (1999) 4964, astro-ph/9810479.
[14] C. Akerlof, et al., Nature 398 (1999) 400, astro-ph/9903271; M.S. Briggs, et al., astro-ph/9903247.
[15] S.D. Biller, et al., Phys. Rev. Lett. 83 (1999) 2108, gr-qc/9810044.
[16] D. Babusci, G. Giordano, G. Matone, Phys. Lett. B 355 (1995) 1.
[17] V.A. Kostelecky, M. Mewes, Phys. Rev. Lett. 87 (2001) 251304, hep-ph/0111026.
[18] V.G. Gurzadian, A.T. Margarian, Phys. Scr. 53 (1996) 513.
[19] D.P. Barber, et al., Nucl. Instrum. Methods A 329 (1993) 79.
[20] M. Lomperski, DESY-93-045.
[21] J. Andruszkow, et al., ZEUS Luminosity Monitor Group Collaboration, DESY-92-066.
[22] I.F. Ginzburg, G.L. Kotkin, S.L. Panfil, V.G. Serbo, V.I. Telnov, Nucl. Instrum. Methods A 219 (1984) 5.
[23] G. Shapiro, et al., LBL-34318 Presented at 1993 Particle Accelerator Conference (PAC 93), Washington, DC, 17–20 May, 1993.
[24] R.C. King, SLAC-0452.